ENSO feedbacks in the IPCC-AR4 models

***Belmadani Ali*[1,2], *DewitteBoris*[1,2,3]**

[1] *Université de Toulouse; UPS (OMP-PCA); LEGOS, 14 Av. Edouard Belin, F-31400 Toulouse, France*
[2] *IRD; LEGOS, F-31400 Toulouse, France*
[3] *IMARPE; Esq. Gamarra y Gal. Valle S/N Chucuito, Callao, Peru*

The dynamics of the ENSO phenomenon are driven by the combination of coupled ocean-atmosphere feedbacks that either amplify or damp the associated oceanic and atmospheric anomalies. Here we focus on two main feedbacks that contribute to the growth or decay of SST anomalies in the equatorial Pacific: the zonal advective feedback that favours short surface-driven ENSO cycles, and the thermocline feedback that induces long recharge oscillator-like ENSO cycles. Whereas several studies relied on statistical approaches to derive the dominant feedback process in IPCC-class climate models, a new methodology is proposed which is based on the use of a simple dynamical model of the tropical Pacific. Results suggest that biases in the representation of the zonal advective and thermocline feedbacks in coupled models are caused by errors in the mean circulation characteristics. Consistently with theory, it is shown that models dominated by the zonal advective feedback (respectively the thermocline feedback) are associated with shorter (respectively longer) oscillations. Differences with previous studies are assessed, and implications for the study of the impact of global warming on ENSO are discussed.

1. INTRODUCTION

The El Niño-Southern Oscillation (ENSO) is the dominant mode of climate variability at interannual time scales, known for its large impacts on the regional climate in many parts of the world. The name «El Niño» (which means child Jesus) was originally given by fishermen from Peru and Ecuador to episodes of anomalously warm surface waters affecting the West coast of South America and occurring from time to time around Christmas (hence the name). Today, it is known as a large-scale warming of the tropical Pacific Ocean occurring every 2 to 7 years and alternating with a cold phase called «La Niña». Thanks to the early observational and

theoretical works by Bjerknes (1966, 1969), it is also known that such fluctuations of the sea surface temperature of the Pacific Ocean are accompanied by dramatic basin-wide changes in sea level pressure, called «the Southern Oscillation». Since then, these events have been understood as a coupled ocean-atmosphere phenomenon called ENSO. Understanding the physical mechanisms driving the ENSO cycle is of great importance for most societies because of its worldwide impacts. Surrounding countries of the Pacific Ocean are the most vulnerable: during the strong 1997–98 El Niño event for instance, the arid western South American coastline was experiencing heavy rainfall and dramatic floodings, as well as a sudden drop of anchovy catches, whereas drought and forest fires were spreading over the normally humid regions of Indonesia and northern Australia. Such natural catastrophes strongly perturb marine and terrestrial ecosystems as well as human activities including agriculture and fisheries (Barber and Chavez, 1983), highlighting the need for efficient tools to predict El Niño and La Niña events on time scales going from seasonal to decadal and multi-decadal. Because of the existence of large-scale atmospheric teleconnections between the tropical Pacific and many other regions of the world, ENSO is also able to affect climate at the global scale. Possible changes in the structure and behaviour of ENSO under global warming are thus likely to induce changes in the world climate and possibly sustain additional positive/negative feedbacks to the global warming trend induced by radiative forcing that remain unpredicted so far.

In order to address these issues, Coupled General Circulation Models (CGCMs) have made much progress during the recent years in the representation of ENSO (AchutaRao and Sperber, 2002; 2006; Joseph and Nigam, 2006). The CMIP3 multi-model dataset, which was collected for the needs of the Intergovernmental Panel on Climate Change Fourth Assessment Report (IPCC-AR4), gathers the latest generation of CGCMs (Meehl et al., 2007a). Most CMIP3 models are able to represent ENSO-like variability (van Oldenborgh et al., 2005; Capotondi et al., 2006; Guilyardi, 2006; Belmadani et al., 2009), with frequencies within the observed 2-7 years range and a reasonable representation of Sea Surface Temperature (SST) anomalies over the eastern tropical Pacific (AchutaRao and Sperber, 2006). However, they are still subject to many errors in both the simulated ENSO variability (amplitude, frequency, regularity, asymmetry, spatial distribution) and the simulated background climate (see Guilyardi et al., 2009 for a review on these topics). The latter was shown to have a strong influence on characteristics of the ENSO mode

including its amplitude and frequency (An and Jin, 2001; Fedorov and Philander, 2001; Wang and An, 2001), through its contribution to the different feedbacks that control the ENSO cycle.

Indeed, thanks to extensive theoretical work conducted since the 1960s, it is now commonly admitted that ENSO results from the combination of different positive and negative feedback mechanisms that contribute to the amplification or damping of associated anomalies. The main positive feedback is the so-called 'Bjerknes feedback' (Bjerknes, 1969): positive (resp. negative) SST anomalies in the cold tongue region tend to reduce (resp. increase) the zonal SST gradient which in turn lead to weaker (resp. stronger) trade winds that induce positive (resp. negative) thermocline anomalies propagating eastward as downwelling (resp. upwelling) equatorial Kelvin waves towards the eastern tropical Pacific where they contribute to the positive (resp. negative) anomalies via upwelling. Four main theories for ENSO have then been proposed to identify the negative feedbacks responsible for the transition from a warm phase (El Niño) to a cold phase (La Niña) and back: the delayed oscillator involving the reflection of equatorial Rossby waves of the opposite sign at the western boundary (Suarez and Schopf, 1988; Schopf and Suarez, 1988; Battisti and Hirst, 1989), the western Pacific oscillator in which the trade winds force equatorial Kelvin waves of the opposite sign, as a result of anticyclonic circulation off the equator due to off-equatorial cold SST anomalies induced by Rossby waves (Weisberg and Wang, 1997), the advective-reflective oscillator whereby fluctuations of the edge of the warm pool are driven by anomalous zonal advection (Picaut et al., 1997) and the recharge oscillator which emphasizes the equatorial recharge/discharge processes due to Sverdrup transport (Jin, 1996; 1997a,b). These theories are complementary in the sense that they may be combined in different ways to understand the observed diversity of ENSO events (Jin and An, 1999; Fedorov and Philander, 2000; An and Jin, 2001). Several studies have focused on the respective role of two main positive feedbacks – that contribute to the Bjerknes feedback – on ENSO as simulated by simple and intermediate coupled models of the tropical Pacific: the zonal advective feedback and the thermocline feedback (Hirst, 1986; Jin and An, 1999; An and Jin, 2001; Fedorov and Philander, 2001).

Indeed, surface wind stress has an effect on both zonal advection of mean SST by anomalous zonal currents in the central Pacific (the zonal advective feedback), and the vertical advection of subsurface temperature by the mean upwelling in the eastern Pacific (the thermocline feedback). Both feedbacks are important terms of the heat budget of the mixed layer in the tropical Pacific (Hirst, 1986). Depending on the longitudinal posi-

tion of wind anomalies, the zonal advective feedback favors the transition or the growth of the ENSO cycle and consequently sustains short 2–4 years or long 4–6 years oscillations with low or high amplitude (An and Wang, 2000; Wang and An, 2001). On the other hand, the thermocline feedback is controlled by vertical displacements of the thermocline as a result of the basin-wide adjustment of the ocean to wind variations. It is responsible for high amplitudes and long ENSO timescales (4–6 years) because of an increased time of recharge/discharge of the equatorial heat content, accordingly to the recharge oscillator paradigm (Jin, 1996; 1997a,b). In fact, both feedbacks coexist in nature, which makes ENSO a hybrid coupled mode (Fedorov and Philander, 2000). The balance between the two is therefore a key parameter in the determination of the structure and dynamics of ENSO and the period of the ENSO cycle. An and Jin (2001) and Fedorov and Philander (2001) further showed that the combined effect of both mechanisms on ENSO dynamics is sensitive to the mean state (particularly the intensity of the trade winds, the thermocline depth, the temperature difference across the thermocline, and the mean upwelling), consistently with the observed change in ENSO frequency and amplitude after the late 1970s climate shift (An and Wang, 2000; Wang and An, 2001).

Here we review the main studies that have assessed the strength of these feedbacks in the CMIP3 models and propose a new diagnostic based on dynamical approaches. The paper is organized as follows: section 2 is a review of the existing literature, whereas section 3 is a presentation of the models and datasets as well as the methodologies used to diagnose ENSO feedbacks. Section 4 presents the results obtained with the new methodology. Section 5 is a discussion followed by concluding remarks.

THE ZONAL ADVECTIVE AND THERMOCLINE FEEDBACKS IN CLIMATE MODELS

In an attempt to assess possible changes in ENSO under global warming, van Oldenborgh et al. (2005) diagnosed the strength of coupled ENSO feedbacks in 20th century climate simulations performed with the CMIP3 models, in order to identify those that best reproduce the real world, and then use the obtained model subset to make climate projections. The theoretical background they used is based on the works by Fedorov and Philander (2001) and by Burgers and van Oldenborgh (2003). Two main feedbacks are considered: the thermocline feedback, in which zonal wind stress anomalies force thermocline anomalies that propagate

as equatorial Kelvin and Rossby waves and eventually induce SST anomalies via upwelling and mixing; and the zonal advective feedback, where wind anomalies directly induce SST anomalies through zonal advection, local anomalous upwelling, evaporation and mixed-layer depth anomalies. The SST anomalies caused by the combination of both mechanisms are then able to feedback on the wind forcing, according to Bjerknes (1969)'s mechanism. Note that an extension of the study by van Oldenborgh et al. (2005) was proposed by Philip and van Oldenborgh (2009) so as to include external atmospheric noise and non-linearities. In order to diagnose the effect of thermocline and wind variations on SST, van Oldenborgh et al. (2005) fitted CGCM outputs to a linearized SST equation (Burgers and van Oldenborgh, 2003):

$$\frac{dT}{dt}(x,y,t) = \alpha(x,y)\ \ d_{20}(x,y,t-\delta) + \beta(x,y) \\ \tau_x(x,y,t) - \gamma(x,y)\ \ T(x,y,t) \tag{1}$$

where T is the local SST (°C), α (°C.m^{-1}.month^{-1}) parametrizes upwelling and mixing of thermocline depth anomalies d_{20} (m), δ is the upwelling time (month), β (°C.Pa^{-1}.month^{-1}) parametrizes zonal advection, upwelling, evaporation and mixed-layer depth variations induced by wind stress anomalies τ_x (Pa), and γ (month^{-1}) is a damping term including the effect of cloud and radiative feedbacks.

Values obtained for α and β thereby provide a quantification for respectively the thermocline feedback and the zonal advective feedback, which are intercompared for the CMIP3 multi-model ensemble and assessed against observations from the Tropical Atmosphere-Ocean (TAO) array of moored buoys (McPhaden et al., 1998) covering the 1983-2004 period. The authors find that most models over-estimate the zonal advective feedback (β) whereas they show a thermocline feedback (α) that is comparable to the observations.

On the other hand, Guilyardi (2006) diagnoses the ENSO mode in the CMIP3 models in terms of S-mode (SST mode) and T-mode (thermocline mode), already described by several authors (Hirst, 1986; Neelin et al., 1998; Fedorov and Philander, 2001). To do so, lag-correlation analyses between an index of the zonal SST gradient[1] and an index of SST vari-

[1] The Trans Niño Index (TNI), equal to the difference between the normalized SST anomalies in the Niño1+2 region (90°W-80°W, 10°S-0°N) and the normalized SST anomalies in the Niño4 region (160°E-150°W, 5°S-5°N).

ability[2] (Trenberth and Stepaniak, 2001) allow separating westward and eastward propagations of SST anomalies. Indeed, the direction of propagation is the result of the influence of ocean-atmosphere coupling on equatorial Kelvin and Rossby waves (Hirst, 1986): whereas the zonal advective feedback-related S-mode tends to destabilize the westward propagating Rossby waves and to damp the eastward propagating Kelvin waves, thereby favouring westward propagating SST anomalies, the thermocline feedback-related T-mode destabilizes Kelvin waves and damps Rossby waves, favouring eastward propagating SST anomalies. Consistently with van Oldenborgh et al. (2005), Guilyardi (2006) found that most CGCMs simulate an S-mode or a hybrid mode regime, with few models exhibiting a T-mode.

These statistical approaches propose original diagnostics that appear to be very useful for the community of climate modellers and users, because of the guidance they provide in the identification and interpretation of biases in the simulated mean state and ENSO variability. Yet, they do not explicitly provide any clear physical explanation for the tendency of a model to favour one ENSO regime over the other. Moreover, they neglect non-linearities associated to zonal and vertical advection, though these are known to have a large influence on ENSO variability (Timmermann and Jin, 2002). In order to complement and test the relevance of the studies by van Oldenborgh et al. (2005) and Guilyardi (2006), a different methodology is proposed here: it relies on a simple dynamical ocean model parametrized from the CGCM outputs so as to infer the strength of the ENSO feedbacks and track the mean state biases responsible for the over– or under-estimation of these feedbacks.

3. DATA AND METHODS

3.1. Data

The CMIP3 multi-model ensemble used in this study is presented in table 1. Monthly outputs from the pre-industrial control experiment (concentration of greenhouse gases fixed to 1850 estimates) are used to evaluate the modelled ENSO under past/present climate. Model outputs are compared to monthly outputs from the SODA 1.4.2 global ocean reanalysis over 1958-2001 (Carton and Giese, 2008). It consists in the Parallel

[2] The Niño3-SST index, equal to the normalized SST anomalies in the Niño3 region (150°W-90°W, 5°S-5°N).

Ocean Program (POP – Smith et al., 1992) Ocean General Circulation Model (OGCM) with 0.25°x0.4° horizontal resolution and 40 vertical levels, constrained by data assimilation and forced by surface winds and heat fluxes from the European Center for Medium Range Weather Forecasts (ECMWF) ERA-40 atmospheric reanalysis (Uppala et al., 2005). See Carton et al. (2000) and Carton and Giese (2008) for details.

Table 1

Description of the CGCMs considered in this study. The run number is specified if there is more than one ensemble member (different initial conditions). Resolutions are given along the equator. Due to gaps in the data some models show variables with different time spans

Model Number	Model Name	Modelling Group	Atmosphere Resolution	Ocean Resolution	Length of Simulation (yrs)
1	BCCR-BCM2.0	BCCR/NERSC/GFI (Norway)	1°x1°L31	1°x1°L33	155
2	CCCMA-CGCM3.1	CCCMA (Canada)	3.75°x3.71° L31	1.88°x1.86° L29	155
3	CCCMA-CGCM3.1-t63	CCCMA (Canada)	2.81°x2.79° L31	1.41°x0.93° L29	155
4	CNRM-CM3	Météo France/CNRM (France)	2.81°x2.79° L45	2°x1°L33	150
5	CSIRO-MK3.0 (run1)	CSIRO (Australia)	1.88°x1.86° L18	1.88°x0.93° L31	134
6	CSIRO-MK3.5	CSIRO (Australia)	1.88°x1.86° L18	1.88°x0.93° L31	134
7	GFDL-CM2.0	NOAA GFDL (USA)	2.5°x2°L24	1°x0.33°L50	129 (U) 150 (T,S,SST,τ)
8	GFDL-CM2.1	NOAA GFDL (USA)	2.5°x2.02° L24	1°x0.33°L50	150
9a	GISS-AOM (run1)	NASA/GISS (USA)	4°x3°L12	4°x3°L31	155
9b	GISS-AOM (run2)	NASA/GISS (USA)	4°x3°L12	4°x3°L31	155
10	GISS-MODEL-E-H	NASA/GISS (USA)	5°x4°L20	1°x1°L33	125
11	GISS-MODEL-E-R	NASA/GISS (USA)	5°x4°L20	5°x4°L33	104

Continued tabl. 1

Model Number	Model Name	Modelling Group	Atmosphere Resolution	Ocean Resolution	Length of Simulation (yrs)
12	IAP-FGOALS1.0-g (run1)	LASG/IAP (China)	2.81°x2.79° L26	1°x1°L33	155
13	INGV-ECHAM4	INGV (Italy)	1.125°x1.12 °L19	1°x1°L33	100
14	INM-CM3.0	INM (Russia)	5°x4°L21	2.5°x2°L33	134
15	IPSL-CM4	IPSL (France)	3.75°x2.54° L19	2°x1°L31	147
16	MIROC3.2-HIRES	CCSR/NIES/FRCGC (Japan)	1.125°x1.12 °L56	1.125°x0.56° L33	100
17	MIROC3.2-MEDRES	CCSR/NIES/FRCGC (Japan)	2.81°x2.79° L20	1.41°x0.56° L33	150
18	MIUB-ECHO-G	MIUB (Germany)	3.75°x3.71° L19	2.81°x0.5° L20	147
19	MPI-ECHAM5	MPI (Germany)	1.88°x1.87° L32	1°x1°L40	123
20	MRI-CGCM2.3.2A	MRI (Japan)	2.81°x2.79° L30	2.5°x0.5°L23	154
21	NCAR-CCSM3.0 (run2)	NCAR (USA)	1.41°x1.40° L26	1.125°x0.27° L40	150
22	UKMO-HadCM3 (run1)	Met Office (UK)	3.75°x2.5°L 19	1.25°x1.25° L20	148
23	UKMO-HadGEM1	Met Office (UK)	1.875°x1.25 °L38	1°x0.34°L40	78 (U,T,S) 147 (SST,τ)

3.2. Methods

The spatial and temporal structure of ENSO was diagnosed from the results of the Singular Value Decomposition (SVD; Bretherton et al., 1992) between the SST and wind stress anomalies in the tropical Pacific Ocean (11°S–11°N) over the whole available time span (table 1). Anomalies are relatively to monthly model climatology. The period of ENSO is defined as the period associated to the dominant significant peak in the [1–10] years frequency band of the Fast Fourrier Transform (FFT) power spectrum of the first SVD mode time serie associated to SST anomalies. The significance of the detected peaks was assessed against red noise

level with the same lag-1 autocorrelation. Note that the lag-1 autocorrelation values obtained within the model ensemble were not high enough to approximate red noise spectra within the low-frequency band with squared power laws. Confidence levels were assessed against a chi-square distribution with two degrees of freedom (Torrence and Compo, 1998). The spectrum was computed by ensemble-averaging the spectra obtained from a 20-year running window (15 years for SODA that spans a shorter period) with a 50% overlapping factor and hann filtering, in order to achieve statistical significance. Results are presented for some models in figure 1, whereas the ENSO period estimates (and the associated confidence levels) are specified for the whole dataset in table 2. Consistently with previous studies (van Oldenborgh et al., 2005; Capotondi et al., 2006; Guilyardi, 2006), although most CGCMs are able to capture ENSO-like variability, the spatial patterns for wind stress and SST anomalies as well as the associated frequencies are heterogeneous among the dataset: from 2.0 years (CSIRO-MK3.0, MIUB-ECHO-G, MRI-CGCM2.3.2A) to 5.0 years (CSIRO-MK3.5, GFDL-CM2.1), SODA showing a typical ENSO period of 3.7 years. The spectra exhibit a variety of shapes, from a narrow band centered around the main peak of interannual variability (CNRM-CM3, MIUB-ECHO-G) to a wide multi-peak spectrum (UKMO-HadCM3). Consistently with van Oldenborgh et al. (2005) and Guilyardi (2006), seven models do not exhibit any significant peak in the interannual frequency band: CCCMA-CGCM3.1 (T47), CCCMA-CGCM3.1 (T63), GISS-AOM (run 1 & 2), GISS-MODEL-E-H, GISS-MODEL-E-R, MIROC3.2-HIRES, MIROC3.2-MEDRES. For this reason, only the 16 CGCMs listed in bold fonts in table 2 were considered in the rest of the study.

Table 2

ENSO Periods of the models

Model Name	ENSO Period (yrs)	Confidence Level (%)	Model Name	ENSO Period (yrs)	Confidence Level (%)
SODA 1.4.2	3.7	80	GISS-MODEL-E-R	–	–
			IAP-FGOALS1.0-g (run1)	3.3	95
BCCR-BCM2.0	4.0	63	INGV-ECHAM4	4.0	85
CCCMA-CGCM3.1	–	–	INM-CM3.0	3.3	85

Continued tabl. 2

Model Name	ENSO Period (yrs)	Confidence Level (%)	Model Name	ENSO Period (yrs)	Confidence Level (%)
CCCMA-CGCM3.1-t63	–	–	IPSL-CM4	2.5	95
CNRM-CM3	3.3	95	MIROC3.2-HIRES	–	–
CSIRO-MK3.0 (run1)	2.0	95	MIROC3.2-MEDRES	–	–
CSIRO-MK3.5	5.0	90	MIUB-ECHO-G-ECHO-G	2.0	95
GFDL-CM2.0	3.3	80	MPI-ECHAM5	4.0	85
GFDL-CM2.1	5.0	95	MRI-CGCM2.3.2A	2.0	95
GISS-AOM (run1)	–	–	NCAR-CCSM3.0 (run2)	2.2	95
GISS-AOM (run2)	–	–	UKMO-HadCM3 (run1)	2.9	95
GISS-MODEL-E-H	–	–	UKMO-HadGEM1	4.0	75

A simple dynamical model of the tropical Pacific is used with prescribed wind forcing and a linearization of the ocean dynamics around a mean oceanic state derived from the CGCMs, in order to compute explicitly the contribution of the advection terms of the SST equation, including non-linearities, and thereby quantify objectively the strength of the zonal advective and thermocline feedbacks. The main advantages include:

– to provide a simple way to perform a heat budget for the CMIP3 models, which would require the manipulation of large datasets (3D temperature and currents) if based on the direct CGCM outputs;

– to get estimates of vertical velocities, which remain difficult to obtain from the direct model outputs because of the low signal-to-noise ratio for this field in most CGCMs;

– to provide a method for comparing models with different characteristics (resolution and mixing scheme among others);

– to evaluate for each CGCM to which degree its tropical ocean variability can be considered a 'linear' response to the wind forcing.

The tropical Pacific model is the oceanic component of an Intermediate Coupled Model (ICM) named LODCA (Linear Ocean Dynamically Coupled to Atmosphere – Dewitte, 2000). For clarity we will simply refer to the model as 'LODCA'. It is an extension of the oceanic component of the CZ model (Zebiak and Cane, 1987) with three baroclinic modes

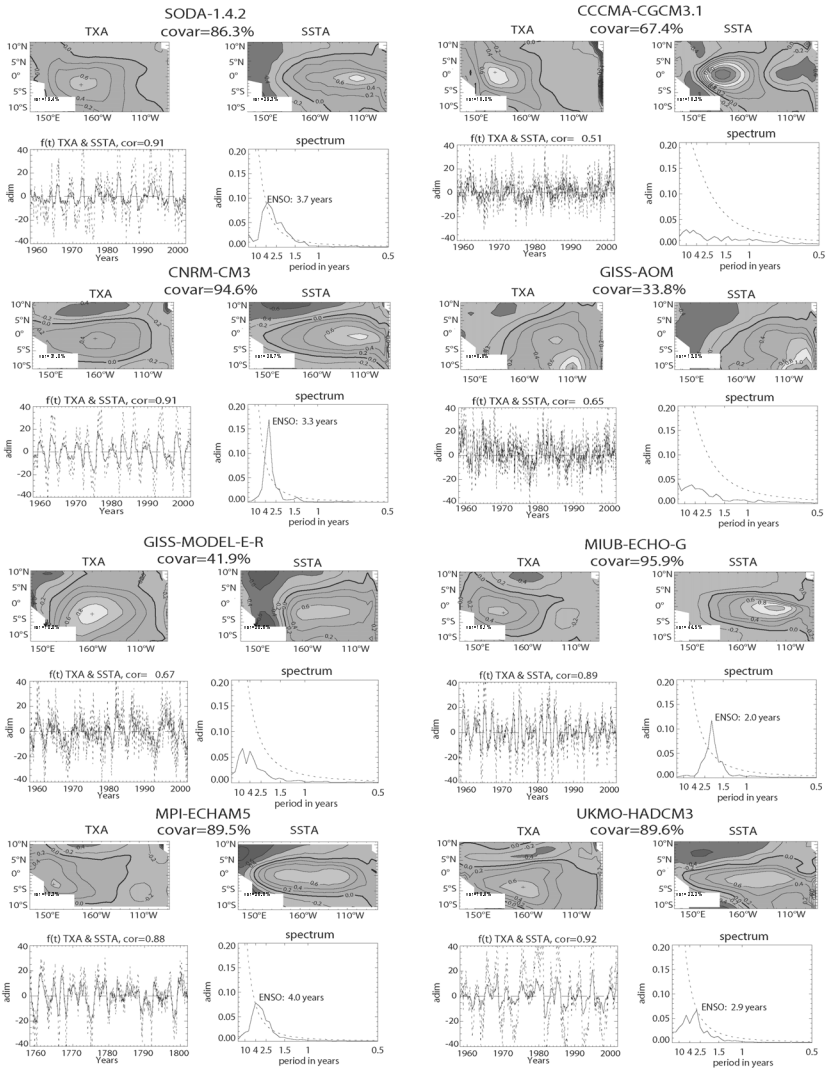

Fig. 1. First SVD mode between wind stress anomalies and SST anomalies (11°S-11°N, 135°E-80°W):

(a) SODA 1.4.2, **(b)** CCCMA-CGCM3.1 (T47), **(c)** CNRM-CM3, **(d)** GISS-AOM (run2), **(e)** GISS-MODEL-E-R, **(f)** MIUB-ECHO-G, **(g)** MPI-ECHAM5, **(h)** UKMO-HadCM3. For each model, from left to right and top to bottom: spatial patterns for the anomalies of respectively zonal wind stress and SST, associated adimensionalized time series (full line for SST anomalies, dashed line for wind stress anomalies), and the corresponding frequency spectra adimensionalized by the energy integrated over the whole frequency domain (full line for SST, dashed line for confidence levels). CI = 0.2 units. Spatial patterns are adimensionalized by their

instead of one. The circulation is driven by adiabatic, linear shallow-water wave dynamics. It includes three baroclinic modes characterized by their respective phase speeds c_n, wind projection coefficients P_n, friction coefficients r_n, and thermocline coefficients $scl_n(z)$ that weight the different sea level baroclinic contributions to thermocline displacements – see Dewitte (2000) for details. Values for these parameters are prescribed to those obtained from a baroclinic mode decomposition of the mean stratification performed for each of the IPCC models at the location (along the equator) of the maximum variability of the zonal wind stress anomaly pattern associated to the first SVD mode between SST and wind stress anomalies (see above), where the impact of the wind forcing on the ocean dynamics is the strongest at interannual timescales. Climatological velocity and SST fields are also prescribed to those from the CGCMs, in order to complete the procedure that allows fitting the mean oceanic state of LODCA to that of each of the CGCMs.

Like in Zebiak and Cane (1987), SST anomalies are computed from a non-linear mixed layer temperature equation that considers mostly large scale zonal and vertical advections (Dewitte, 2000):

$$\frac{\partial T'}{\partial t} = -u'(\overline{T}+T')_x - \overline{u}(T')_x - v'(\overline{T}+T')_y - \overline{v}(T')_y$$

$$-\gamma.\{M(\overline{w}+w') - M(\overline{w})\}\overline{T}_z \quad -\gamma.M(\overline{w}+w')\frac{T'-T'_{sub}(h',\overline{h})}{H_{mix}} - \alpha T' \quad (2)$$

M(x) is a step function: M(x)=x if x≥ 0 ; M(x)=0 if x<0. T', (u', v', w') and h' stand for the anomalies for SST, surface currents and thermocline displacements respectively. Barred quantities represent climatological fields. T_{sub} is for subsurface temperature at the base of the mixed layer and is parameterized as in Dewitte and Périgaud (1996). x, y and z indices stand for the partial derivatives according to the respective spatial coordinates. γ is an efficiency factor relating entrainment to upwelling, and varies from west to east between the values of 0.5 and 1.0 in order to take the effect of a zonally varying mixed-layer depth into account (see Dewitte,

respective variance over the domain and multiplied by 10. The location of maximum variance in wind stress anomalies is indicated by a cross on the map of the associated SVD mode. Percentage of explained variance for SST and zonal wind stress are indicated on the corresponding panels. Percentage of explained covariance is also provided. Correlation value between time series is indicated above the corresponding panel and the dominant ENSO period is mentioned on the spectrum plot if significant. Confidence levels for each model are specified in table 2. The 95% confidence level is plotted in (b), (d) and (e)

2000). α is a damping coefficient equal to (115 days)$^{-1}$. $-u'(\overline{T}+T')_x$ is for zonal advection of temperature by the zonal current anomalies, and $-\overline{u}(T')_x$ is for zonal advection of temperature anomalies by the mean zonal currents. $-v'(\overline{T}+T')_y$ and $-\overline{v}(T')_y$ are for the meridional counterparts. $-\gamma.\{M(\overline{w}+w')-M(\overline{w})\}\overline{T}_z$ is for vertical entrainment of mean temperature across the thermocline by the vertical current anomalies and is only for upwelling. $-\gamma.M(\overline{w}+w')\dfrac{T'-T'_{sub}(h',\overline{h})}{H_{mix}}$ is for vertical entrainment of temperature anomalies across the thermocline by the total upwelling. For simplicity the latter two terms will be respectively referred to as $-w'.(\overline{T})_z$ and $-w.(T')_z$ in the rest of the paper. $-\alpha T'$ is a Newtonian damping term which includes the contribution of surface heat flux anomalies.

Table 3

Comparison between CGCM and LODCA outputs

Model Name	Niño3-SST (LODCA & CGCM)	
	Correlation	RMS difference (°C)
SODA 1.4.2	0.85	0.76
BCCR-BCM2.0	0.89	0.57
CNRM-CM3	0.96	0.84
CSIRO-MK3.0 (run1)	0.86	0.57
CSIRO-MK3.5	0.89	0.40
GFDL-CM2.0	0.87	0.44
GFDL-CM2.1	0.85	0.78
IAP-FGOALS1.0-g (run1)	0.96	0.57
INGV-ECHAM4	0.94	0.34
INM-CM3.0	0.90	0.51
IPSL-CM4	0.94	0.41
MIUB-ECHO-G	0.89	0.62
MPI-ECHAM5	0.77	0.78
MRI-CGCM2.3.2A	0.82	0.48
NCAR-CCSM3.0 (run2)	0.90	0.40
UKMO-HadCM3 (run1)	0.93	0.58
UKMO-HadGEM1	0.86	0.42

The linear model is forced with wind stress anomalies from the IPCC models, in order to fit its dynamics to the equatorial dynamics of the CGCMs and derive SST anomalies together with the tendency terms of

the SST equation. The main advantage in comparison to a model using only one baroclinic mode like the CZ model is that it better represents equatorial Kelvin and Rossby wave dynamics. In particular, wave dissipation is not only taken into account through a Rayleigh-type friction but through vertical propagation of energy (Dewitte and Reverdin, 2000). Hence we expect to better represent with LODCA the contribution of the ENSO feedbacks on the rate of SST change. The simulated SST anomalies from LODCA are compared to the direct CGCM outputs. The Niño3-SST index shows a good agreement between LODCA and the CGCMs (table 3). The differences between the anomalies simulated by LODCA and those simulated by the CGCMs may be due to a number of processes: these include some non-linearities present in the CGCMs but not in LODCA (the latter only accounts for non-linear advection associated to long equatorial waves), the reflection of equatorial waves (LODCA having an idealized meridional coastline with no through-flow), the dispersion and dissipation processes associated to thermocline variability (LODCA having a steady homogeneous thermocline), or the surface heat fluxes which are very simply parameterized in LODCA. Nevertheless, results from table 3 indicate that the variability of most models can be accounted for to a large extent by linear ocean dynamics. In the following section, results based on the LODCA simulations are used to classify the models according to the main ENSO regime.

4. RESULTS

4.1. Model errors in the advection terms

In the rest of the study, the variability of the tendency terms are assumed to provide estimates of the strength of the different ENSO feedbacks, and deviations from the results obtained with LODCA fitted to SODA are expected to reflect the tendency of the CGCMs towards one feedback regime or the other. Figure 2 presents the deviation of the variability (RMS) for the zonal and vertical advection terms respectively in the western/central Pacific and in the eastern Pacific, relatively to SODA for the 16 CGCMs. For simplicity, we will refer as «departure» the deviation from SODA hereafter, unless specified. A detailed examination allows quantifying which terms account the most for the departures in total zonal/vertical advection. In particular, mean zonal advection of anomalous temperature ($-\overline{u}.(T')_x$ -dark bars) can be significantly larger or

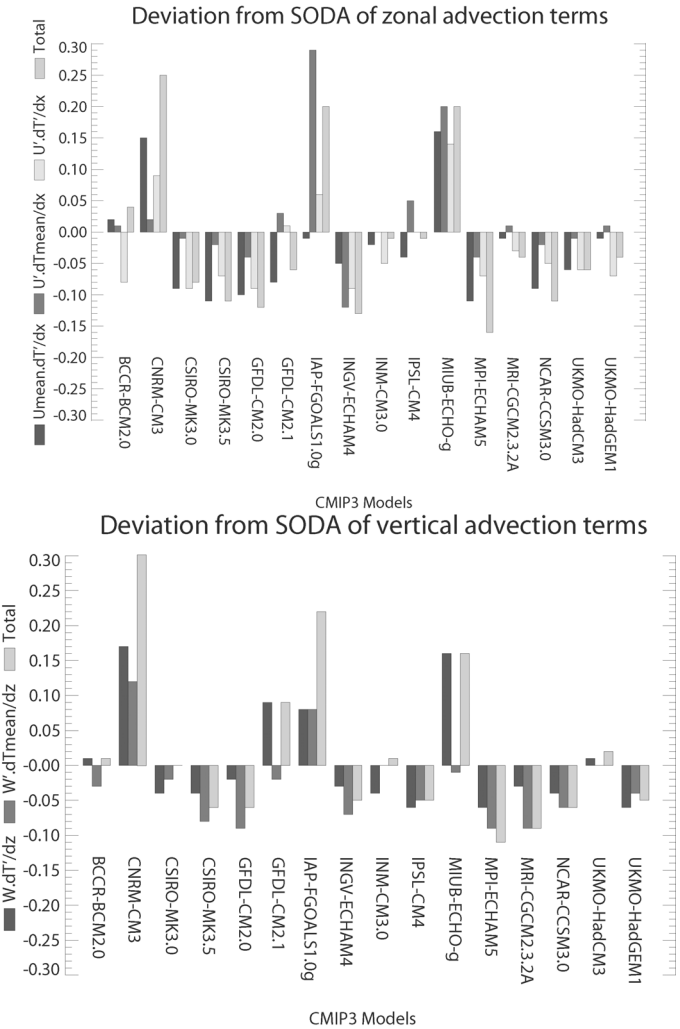

Fig. 2. Histogram of the deviation in the variability (RMS) of the advection terms (relatively to SODA) for the CMIP3 models: (top panel) zonal advection terms averaged in the Niño4eq region and (bottom panel) vertical advection terms averaged in the Niño3eq region. Units are °C/month

smaller for the CMIP3 models than for SODA, with a tendency towards a similar deviation from SODA to that of total zonal advection (grey bars). Similarly, the departure in mean vertical advection of anomalous temperature is comparable to the departure in total vertical advection. Table 4 presents for each advection term the number of models that have a departure (relatively to different references) of the same sign/order of magnitude ($^{+}$/– 50% of the value) as that of the sum of the zonal/vertical advection terms: whatever the chosen reference, zonal/vertical advection by the mean currents are the most representative terms to account for the departures in total zonal/vertical advection, and thus can be considered «proxies» of the tendencies of the CGCMs to favour one feedback over the other.

Table 4

Number of CGCMs with departures in tendency terms representative of the departure for total zonal/vertical advection

Departures in	have the:	Same sign as departure for total zonal/vertical advection		Same order of magnitude as departure for total zonal/vertical advection	
tendency terms	relatively to:	SODA	Ensemble Mean	SODA	Ensemble Mean
$-\overline{u}.(T')_x$		15	13	10	11
$-u'.(\overline{T})_x$		11	12	3	8
$-u'.(T')_x$		13	13	7	5
$-w.(T')_z$		14	15	11	10
$-w'.(\overline{T})_z$		10	14	9	6

4.2. ENSO feedbacks in CGCMs

In order to assess the balance between the zonal advective feedback and the thermocline feedback in the CGCMs, the variability of $-w.(T')_z$ averaged in the Niño3eq region (150°W-90°W, Eq.) is represented in figure 3 as a function of the variability of $-\overline{u}.(T')_x$ averaged in the Niño4eq region (160°E-150°W, Eq.). Interestingly, there is no clear linear relationship between the two advection terms among the models, illustrating the diversity of behaviour in the model ensemble in terms of the privileged ENSO regime. The CGCMs are gathered around the ensemble mean with

models overestimating mean zonal advection (star group) and models overestimating mean vertical advection (circle group). In between, a few models exhibit a balance between advection terms that is comparable to the ensemble mean (square group). SODA also belongs to this category, though having larger zonal advection than the ensemble mean. In order to

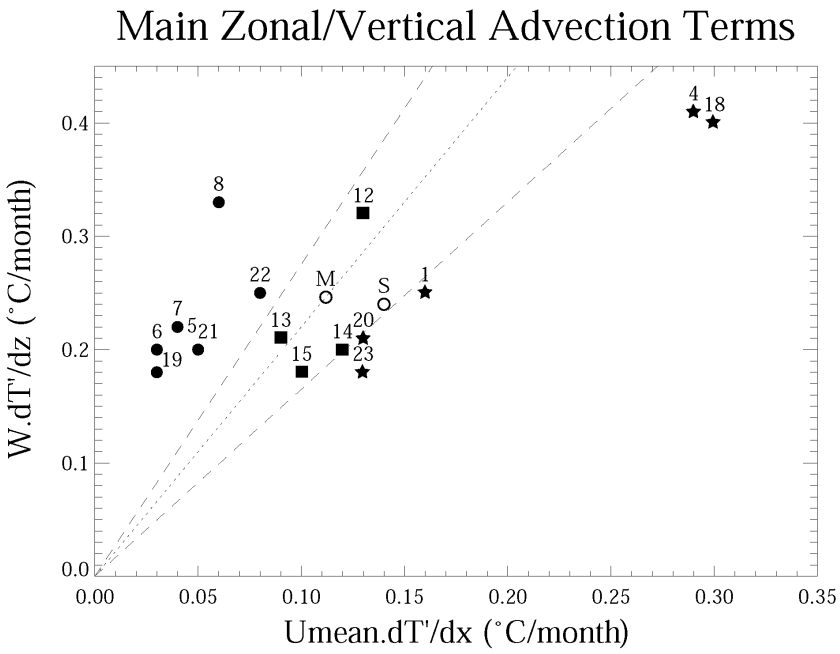

Fig. 3. Scatterplot of the RMS of vertical advection of anomalous temperature by the total vertical currents $-w.(T')_z$ vs. the RMS of zonal advection of anomalous temperature by the mean zonal currents $-\bar{u}.(T')_x$ for the CMIP3 models. $-w.(T')_z$ (resp. $-\bar{u}.(T')_x$) is averaged in the Niño3eq (resp. Niño4eq) region.

The dotted line has a slope equal to the mean value of $-w.(T')_z / \bar{u}.(T')_x$, and the dashed lines have slopes equal to +/-25% of the slope of the dotted line. Model symbols correspond to their positions relative to the dashed lines: squares between them, stars on their right hand side and filled circles on their left hand side. Unfilled circles are for the references: S stands for SODA and M stands for the multi-model ensemble mean. Model names are referenced in table 1. Note that CSIRO-MK3.0 and NCAR-CCSM3.0 have the same position. Units are °C/month

assess to which extent the ratio between $-w.(T')_z$ and $-\overline{u}.(T')_x$ is controlled by the mean state and more specifically by the mean circulation, a similar figure is presented, considering only the mean zonal and vertical currents (figure 4). Interestingly, the scatter plot exhibits a distribution of the balance between zonal and vertical movements among the models that is similar to figure 3 but emphasizes the differences between models.

Again three groups of models can be distinguished: the models located on the left of the flattest dashed line have strong mean equatorial zonal currents relatively to mean equatorial upwelling, in comparison to SODA. Thus these CGCMs can be considered as dominated by the zonal advective feedback (group 1). Similarly, the models located on the right

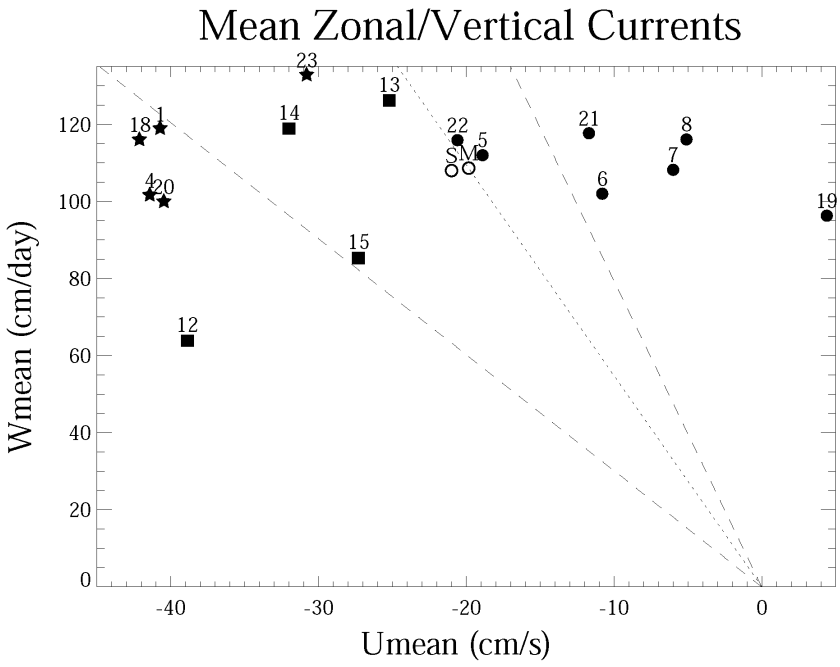

Fig. 4. Scatterplot of the mean vertical currents $\overline{w}$ (averaged over Niño3eq) vs. the mean surface zonal currents $\overline{u}$ (averaged over Niño4eq) for the CMIP3 models.

The dotted line has a slope corresponding to the multi-model ensemble mean and the dashed lines have slopes corresponding to +/-45% of the slope of the dotted line. Symbols are from fig. 3. Model names are referenced in table 1. Units for zonal (resp. vertical) currents are cm.s^{-1} (resp. cm.day^{-1}).

of the steepest dashed line can be considered as dominated by the thermocline feedback (group 3). The models located between the dashed lines have a fairly reasonable balance between zonal advective and thermocline feedbacks (group 2), with a $\overline{w}/\overline{u}$ ratio comprised in the arbitrarily chosen range of the multi-model mean $\overline{w}/\overline{u}$ ratio +/– 45%. Only four models are classified differently by figure 3 and figure 4: CSIRO-MK3.0, IAP-FGOALS1.0-g, UKMO-HadCM3 and UKMO-HadGEM1. Moreover, the latter two exhibit a stronger relative importance of vertical movements than the other models from the hybrid group and the reference (figure 4), which is consistent with the results of figure 3. It was checked that considering SODA as the reference instead of the mean value over the multi-model ensemble leads to the same classification for all models, as it exhibits a dynamical regime very similar to that of the ensemble mean. Noteworthy, the choice of the reference only determines the limits between the different groups of models, and does not affect the differences among the CGCMs in regard to the relative importance of zonal and vertical advection terms in the heat budget.

To summarize, we have identified from the heat budget of each CGCM that biases in the simulated mean surface circulation ($\overline{u},\overline{w}$) can be used to classify the CGCMs in groups relevant to their dominant ENSO regime.

4.3. Impact on the ENSO timescale

In the following, we investigate to which extent characteristics of the ENSO mode can be related to the biases in the mean state identified above: as detailed in the introduction, according to several studies (*e.g.* Wang and An, 2001; Fedorov and Philander, 2001), it is expected that models with a dominant zonal advective feedback (resp. thermocline feedback) have a short (resp. long) ENSO period.

Figure 5 presents the ENSO periods (table 2) for the CGCMs classified according to the dominant feedback. Consistently with earlier studies (Fedorov and Philander, 2001; van Oldenborgh et al., 2005; Guilyardi, 2006), models dominated by the zonal advective feedback have a tendency to simulate a shorter ENSO cycle (2.7 years on average) than those dominated by the thermocline feedback (4.3 years). The mean ENSO period for group 2 lies in between (2.9 years), but is closer to the value for group 1. One possible explanation is the arbitrary definition of the limits

between groups (see previous section). However, the fact that the hybrid group follows the general tendency relating the length of the ENSO cycle to the relative strength of the thermocline feedback tends to confirm our results. Note that the period derived from SODA (3.7 years) is higher than that of group 2, but smaller than that of group 3. Considering that the

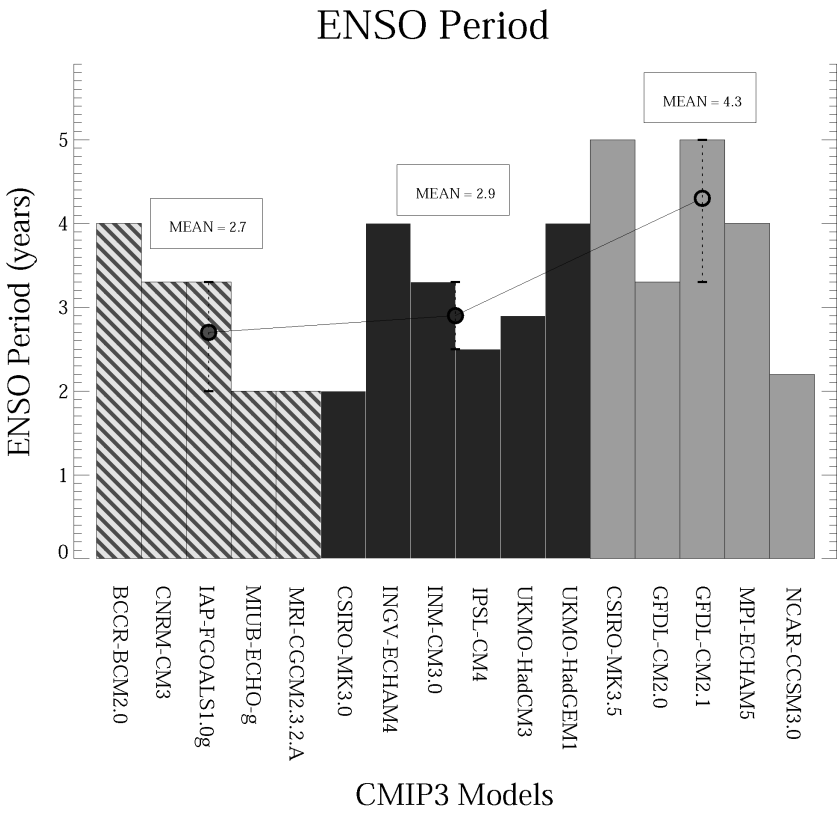

Fig. 5. Histogram of the ENSO period of the CMIP3 models.
Hatched bars are for models with a dominant zonal advective feedback, dark bars are for models with a hybrid feedback and light grey bars are for models with a dominant thermocline feedback. For each group, the black-circled dot represents the mean ENSO period, with value indicated above it. The mean was calculated excluding the models deviating from the mean by more than the standard deviation of the considered group. Error bars are provided that correspond to the highest and lowest values of the models retained for the calculation of the mean value. Units are years.

44-year SODA period comprises a slightly longer record after the 1976 climate shift than before, it might partly explain – together with the tendency of hybrid models towards the higher frequencies – the length of the ENSO timescale. Despite these discrepancies, the results suggest that a realistic representation of ENSO feedbacks leads to realistic timescales of ENSO variability.

Note that other biases might contribute to the heterogeneous periods found within each group. For instance, Yu et al. (2009) showed that the biennial ENSO in NCAR-CCSM3.0 is partly due to biases in the mean Indian Ocean SST and in the Indian and Australian monsoon variability.

5. DISCUSSION AND CONCLUSIONS

As mentioned in section 2., this study is meant to complement those by van Oldenborgh et al. (2005) and Guilyardi (2006). The former study did not explicitly make any model classification, but provided a more qualitative interpretation of model behaviour. In the absence of a clear classification, no relation could be inferred between ENSO feedbacks and periodicity. However, they identified a group of wind-driven models, mainly involving zonal advection, which tend to have a short ENSO cycle. Among them, three models are analyzed by both van Oldenborgh et al. (2005) and the present study (CSIRO-MK3.0, INM-CM3.0, NCAR-CCSM3.0): none of them are classified here as zonal advective feedback-dominated. That is because the feedback loops characterized by van Oldenborgh et al. (2005) do not account for the same processes as the ones identified here, as discussed below.

The main difference between the two studies comes from the formulation of the SST equation: the dynamical model used here explicitly resolves the contributions of the advection terms to SST tendencies (equation (2)), whereas the analysis by van Oldenborgh et al. (2005) is based on the results of a linear statistical model (equation (1)). Wind stress actually induces both horizontal advection in the mixed layer and upwelling across the thermocline, whereas thermocline depth anomalies are subject to upwelling and mixing and are influenced by the wind stress. Hence an enhanced SST sensitivity to wind anomalies for instance (β from equation (1)) does not necessarily lead to a short or to a long ENSO period, as it involves both zonal advective and thermocline feedbacks. In addition, their study neglects non-linearities, which are known to be responsible for El Niño-La Niña asymmetry, extreme El Niño events, low-frequency changes of the mean

state (Timmermann and Jin, 2002; An and Jin, 2004) and interactions between time scales of tropical variability (Dewitte et al., 2007).

On the other hand, seven out of twelve CGCMs that both Guilyardi (2006) and the present study analyze are found to exhibit coherent dynamical regimes, assuming that the separation between S– and T-modes based on the direction of propagation of SST anomalies can provide an estimate of the dominant feedback process. Among these models four are hybrid (INM-CM3.0, IPSL-CM4, UKMO-HadCM3 and UKMO-HadGEM1), that interestingly are among the most realistic models in terms of spatial and temporal ENSO properties (see fig.1 for UKMO-HadCM3). However, no clear relationship is found by Guilyardi (2006) between ENSO frequency and El Niño mode, and only a slight tendency towards lower ENSO frequency for models exhibiting a T-mode is observed. The main differences with the present study are that no subsurface data were considered in Guilyardi (2006) and that the dominant feedback is diagnosed from the direction of propagation of SST anomalies. Most models exhibit an S-mode or a hybrid mode, and even the observations after the 1976 climate shift feature a moderate T-mode, consistently with the observed tendency towards westward propagations before the shift and mixed eastward propagations and standing oscillations after the shift (An and Jin, 2000; Wang and An, 2001). Hence the diagnostic proposed to separate models with an S-mode and models with a T-mode does not allow very marked categories, conversely to the present study (fig.4). In particular, few models exhibit a T-mode, as in theory a dominant thermocline feedback may still be associated to mixed eastward and westward propagation.

Overall this study provides a detailed methodology based on the use of a simplified tropical Pacific model in order to diagnose the dominant mode of interannual variability in complex climate models. It reveals that the main source of error in the CMIP3 model ensemble in regard to the dominant ENSO feedback (zonal advective versus thermocline feedbacks) can be inferred from mean zonal and vertical advection of anomalous temperature. A simple diagnostic based on the mean velocity fields in the surface layer is therefore proposed to classify the models according to the dominant feedback. Consistently with previous studies (Fedorov and Philander, 2001; van Oldenborgh et al., 2005; Guilyardi, 2006), models dominated by the zonal advective (resp. thermocline) feedback have a short (resp. long) ENSO period. Climate models in which ENSO is controlled by a combination of both feedbacks (CSIRO-MK3.0, INGV-ECHAM4, INM-CM3.0, IPSL-CM4, UKMO-HadCM3 and UKMO-

HadGem1) like in the real world are considered the most reliable for climate projections under increasing concentrations of greenhouse gases. The study confirms the need of improving the background climate simulated by IPCC-class models, in order to improve characteristics of simulated interannual variability under past/present climate, and thereby our confidence in climate projections for the 21st century.

The proposed dynamical approach could yield valuable information to study the impact of climate change on ENSO. Indeed, though most CGCMs predict similar changes in the mean state of the tropical Pacific (Liu et al., 2005; van Oldenborgh et al., 2005; Fedorov et al., 2006; Hansen et al., 2006; Vecchi et al., 2006, 2008), including a stronger SST warming at the equator, a reduced zonal SST gradient and a weakened Walker circulation and associated trade winds, no clear changes were reported with regard to ENSO amplitude, frequency or skewness due to the lack of consistency among the different models (van Oldenborgh et al., 2005; Guilyardi, 2006; Merryfield, 2006; Meehl et al., 2007b). However, Guilyardi et al. (2009) point out that process-oriented studies focusing on the feedbacks of the ENSO cycle might allow identifying subsets of more reliable models and possibly clearer changes under a warmer climate. For instance, Guilyardi (2006) showed that the most realistic models in terms of tropical Pacific climatology exhibit an increase of El Niño amplitude under climate change. On the other hand, models identified by van Oldenborgh et al. (2005) as the best with regard to the processes they considered as important for ENSO did not provide any statistically significant result. Because of the similarity of the feedbacks analyzed by the present study and by Guilyardi (2006), and the explicit diagnostic of the ENSO feedbacks which is proposed here, a complete analysis of possible changes in the ENSO feedbacks and the associated mean state characteristics could help understanding changes in ENSO in the model ensemble and possibly identify some consistency among models from the different categories, hybrid models in particular.

Acknowledgements

The authors are thankful to S.-I. An, D. Battisti, J. Boucharel, Y. duPenhoat, E. Guilyardi, F.-F. Jin, M. Lengaigne, S.Y. Philip, and G.J. van Oldenborgh for fruitful discussions, and to S. Bertrand and A. Chaigneau for their help with statistical computation. We acknowledge the modelling groups, the Program for Climate Model Diagnosis and Intercomparison (PCMDI) and the World Climate Research Programme's (WCRP's)

Working Group on Coupled Modelling (WGCM) for their roles in making available the WCRP Coupled Model Intercomparison Project phase 3 (CMIP3) multi-model dataset. Support of this dataset is provided by the Office of Science, U.S. Department of Energy. We would like to thank the Peru Ecosystem Projection Scenarios (PEPS) program of Agence Nationale de la Recherche (ANR) for financial support.

References

1. AchutaRao, K., and K. Sperber, 2002: Simulation of the El Niño-Southern Oscillation: Results from the Coupled Model Intercomparison Project (CMIP). *Climate Dyn.*, **19**, 191–209.

2. ---, and ---, 2006: ENSO simulation in coupled ocean-atmosphere models: are the current models better ? *Climate Dyn.*, **27**, 1–15.

3. An, S.-I., and F.-F. Jin, 2000: An eigen analysis of the interdecadal changes in the structure and frequency of ENSO Mode. *Geophys. Res. Lett.*, **27**, 1573–2576.

4. ---, and B. Wang, 2000: Interdecadal change of the structure of the ENSO mode and its impact on the ENSO frequency. *J. Climate*, **13**, 2044–2055.

5. ---, and F.-F. Jin, 2001: Collective role of thermocline and zonal advective feedbacks in the ENSO mode. *J. Climate*, **14**, 3421–3432.

6. ---, and ---, 2004: Nonlinearity and asymmetry of ENSO. *J. Climate*, **17**, 2399–2412.

7. Barber, R., and F. Chavez, 1983: Biological consequences of El Niño. *Science*, **222**, 203–210.

8. Battisti, D. S., and A. C. Hirst, 1989: Interannual variability in the tropical atmosphere/ocean system: Influence of the basic state and ocean geometry. *J. Atmos. Sci.*, **46**, 1687–1712.

9. Belmadani, A., B. Dewitte, and S.-I. An, 2009: ENSO feedbacks and associated timescales of variability in a multi-model ensemble. *J. Climate*, revised.

10. Bjerknes, J., 1966: A possible response of the atmospheric Hadley circulation to equatorial anomalies of ocean temperature. *Tellus*, **18**, 820–829.

11. ---, 1969: Atmospheric teleconnections from the equatorial Pacific. *Mon. Wea. Rev.,* **97,** 163–172.

12. Bretherton, C. S., C. Smith, and J. M. Wallace, 1992: An intercomparison of methods for finding coupled patterns in climate data. *J. Climate*, **5**, 541–560.

13. Burgers, G., and G. J. van Oldenborgh, 2003: On the impact of local feedbacks in the central Pacific on the ENSO cycle. *J. Climate*, **16**, 2396–2407.

14. Capotondi, A., A. Wittenberg, and S. Masina, 2006: Spatial and temporal structure of tropical Pacific interannual variability in 20th century coupled simulations. *Ocean Mod.*, **15**, 274–298.

15. Carton, J. A., and B. S. Giese, 2008: A reanalysis of ocean climate using Simple Ocean Data Assimilation (SODA). *Mon. Wea. Rev.*, **136**, 2999–3017.

16. ---, G. A. Chepurin, X. Cao, and B. S. Giese, 2000: A Simple Ocean Data Assimilation analysis of the global upper ocean 1950–1995, Part 1: methodology. *J. Phys. Oceanogr.*, **30**, 294–309.

17. Dewitte, B., 2000: Sensitivity of an intermediate coupled ocean-atmosphere model of the tropical Pacific to its oceanic vertical structure. *J. Climate*, **13**, 2363–2388.

18. ---, and C. Périgaud, 1996: El Niño-La Niña events simulated with Cane and Zebiak's model and observed with satellite or in situ data. Part II: model forced with observations. *J. Climate*, **9**, 1188–1207.

19. ---, and G. Reverdin, 2000: Vertically propagating annual and interannual variability in an OGCM simulation of the tropical Pacific in 1985–1994. *J. Phys. Oceanogr.*, **30**, 1562–1581.

20. ---, C. Cibot, C. Périgaud, S.-I. An, and L. Terray, 2007: Interaction between Near-Annual and ENSO modes in a CGCM simulation: Role of the equatorial background mean state. *J. Climate*, **20**, 1035–1052.

21. Fedorov, A. V., and S. G. Philander, 2000: Is El Niño changing ? *Science,* **288**, 1997. doi:10.1126/science.288.5473.1997

22. ---, and ---, 2001: A stability analysis of tropical ocean-atmosphere interactions: bridging measurements and theory for El Niño. *J. Climate,* **14**, 3086–3101.

23. ---, P. S. Dekens, M. McCarthy, A. C. Ravelo, P. B. deMenocal, and M. Barreiro, 2006: The Pliocene paradox (mechanisms for a permanent El Niño). *Science,* **312,** 1485–1489.

24. Guilyardi, E., 2006: El Niño-mean state-seasonal cycle interactions in a multi-model ensemble. *Climate Dyn.*, **26**, 329–348.

25. ---, A. Wittenberg, A. Fedorov, M. Collins, C. Wang, A. Capotondi, G. J. van Oldenborgh, and T. Stockdale, 2009: Understanding El Niño in ocean-atmosphere general circulation models: Progress and challenges. *Bull. Amer. Meteor. Soc.*, **90**, 325–340.

26. Hansen, J., M. Sato, R. Ruedy, K. Lo, D. W. Lea, and M. M. Elizade, 2006: Global temperature change. *Proc. Natl. Acad. Sci.*, **103**, 14288.

27. Hirst, A. C., 1986: Unstable and damped equatorial modes in simple coupled ocean-atmosphere models. *J. Atmos. Sci.*, **43**, 606–630.

28. Jin, F.-F., 1996: Tropical ocean-atmosphere interaction, the Pacific cold tongue, and the El Niño-Southern Oscillation. *Science*, **274**, 76–78.

29. ---, 1997a: An equatorial ocean recharge paradigm for ENSO. Part I: Conceptual model. *J. Atmos. Sci.*, **54**, 811–829.

30. ---, 1997b: An equatorial ocean recharge paradigm for ENSO. Part II: A stripped-down coupled model. *J. Atmos. Sci.*, **54**, 811–829.

31. ---, and S.-I. An, 1999: Thermocline and zonal advective feedbacks within the equatorial ocean recharge oscillator model for ENSO. *Geophys. Res. Lett.*, **26** (19), 2989–2992.

32. Joseph, R., and S. Nigam, 2006: ENSO evolution and teleconnections in IPCC's twentieth-century climate simulations: Realistic representation? *J. Climate,* **19,** 4360–4377.

33. Liu, Z., S. Vavrus, F. He, N. Wen, and Y. Zhong, 2005: Rethinking tropical ocean response to global warming: The enhanced equatorial warming. *J. Climate,* **18,** 4684–4700.

34. McPhaden, M. J., A. J. Busalacchi, R. Cheney, J. R. Donguy, K. S. Gage, D. Halpern, M. Ji, P. Julian, G. Meyers, G. T. Mitchum, P. P. Niiler, J. Picaut, R. W. Reynolds, N. Smith, and K. Takeuchi, 1998: The Tropical Ocean Global Atmosphere (TOGA) observing system: A decade of progress. *J. Geophys. Res.*, **103**, 14169–14240.

35. Meehl, G. A., C. Covey, T. Delworth, M. Latif, B. McAvaney, J. F. B. Mitchell, R. J. Stouffer, and K. E. Taylor, 2007a: The WCRP CMIP3 multimodel dataset: A new era in climate change research. *Bull. Amer. Meteor. Soc.,* **88,** 1383–1394.

36. ---, ---, ---, ---, ---, ---, ---, and ---, 2007b: Global climate projections. *Climate Change 2007: The Physical Science Basis,* S. D. Solomon et al., Eds., Cambridge University Press, 747–845.

37. Merryfield, W. J., 2006: Changes to ENSO under CO_2 doubling in a multimodel ensemble. *J. Climate*, **19**, 4009–4027.

38. Neelin, J. D., D. S. Battisti, A. C. Hirst, F.-F. Jin, Y. Wakata, T. Yamagata, and S. E. Zebiak, 1998: ENSO theory. *J. Geophys. Res.*, 1**03**, 14261–1290.

39. Philip, S. Y., and G. J. van Oldenborgh, 2009: Significant atmospheric nonlinearities in the ENSO cycle. *J. Climate*, accepted, doi: 10.1175/2009JCLI2716.1

40. Picaut, J., F. Masia, and Y. du Penhoat, 1997: An advective-reflective conceptual model for the oscillatory nature of the ENSO. *Science*, **277**, 663–666.

41. Schopf, P. S., and M. J. Suarez, 1988: Vacillations in a coupled ocean-atmosphere model. *J. Atmos. Sci.*, **45**, 549–566.

42. Smith, R. D., J. K. Dukowicz, and R. C. Malone, 1992: Parallel ocean general circulation modeling. *Physica D.*, **60**, 38–61.

43. Suarez, M. J., and P. S. Schopf, 1988: A delayed oscillator for ENSO. *J. Atmos. Sci.*, **45**, 3283–3287.

44. Timmermann, A., and F.-F. Jin, 2002: A nonlinear mechanism for decadal El Niño amplitude changes. *Geophys. Res. Lett.*, **29**, doi:10.1029/2001GL013369.

45. Torrence, C., and G. P. Compo, 1998: A practical guide to wavelet analysis. *Bull. Amer. Meteor. Soc.*, **79**, 1, 61–78.

46. Trenberth, K. E., and D. P. Stepaniak, 2001: Indices of El Niño evolution. *J. Climate*, **14**, 1697–1701.

47. Uppala, S. M., P. W. Kalberg, A. J. Simmons, U. Andrae, V. da Costa Bechtold, M. Fiorino, J. K. Gibson, J. Haseler, A. Hernandez, G. Kelly, X. Li, K. Onogi, S. Saarinen, N. Sokka, R. P. Allan, E. Anderson, K. Arpe, M. A. Balmaseda, A. C. M. Beljaars, L. van den Berg, J. Bidlot, N. Borman, S. Caires, A. Dethof, M. Dragosavac, M. Fisher, M. Fuentes, S. Hagemann, E. Holm, B.J. Hoskins, L. Isaksen, P. A. E. M. Janssen, R. Jenne, A. McNally, J.-F. Mahfouf, J.-J. Mocrette, N. A. Rayner, R. W. Saunders, P. Simon, A. Sterl, K.E. Trenberth, A. Untch, D. Vasiljevic, P. Viterbo, and J. Woollen, 2005: The ERA-40 re-analysis, *Quart. J. Roy.Meteor. Soc.*, **131**, 2961–3012.

48. van Oldenborgh, G. J., S. Y. Philip, and M. Collins, 2005: El Niño in a changing climate : a multi-model study. *Ocean Science*, **1**, 81–95.

49. Vecchi, G. A., B. J. Soden, A. T. Wittenberg, I. M. Held, A. Leetmaa, and M. J. Harrison, 2006: Weakening of tropical Pacific atmospheric circulation due to anthropogenic forcing. *Nature,* **327,** 216–219.

50. ---, A. Clement, and B. J. Soden, 2008: Examining the tropical Pacific's response to global warming. *Eos, Trans. Amer. Geophys. Union,* **89,** 81–83.

51. Wang, B., and S.-I. An, 2001: Why the properties of El Niño changed during the late 1970s. *Geophys. Res. Lett.,* **28,** 3709–3712.

52. Weisberg, R. H., and C. Wang, 1997: A western Pacific oscillator paradigm for the El Niño-Southern Oscillation. *Geophys. Res. Lett.,* **24,** 779–782.

53. Yu, J.-Y., F. Sun and H.-Y. Kao, 2009: Contributions of Indian Ocean and monsoon biases to the excessive biennial ENSO in CCSM3. *J. Climate,* **22**, 1850–1858.

54. Zebiak, S. E., and M. A. Cane, 1987: A model El Niño-Southern Oscillation. *Mon. Wea. Rev.,* **115,** 2262–2278.